A cost and time effective novel methodology to determine specific heat capacity of lithium-ion cells

Journal of Power Sources 500 (2021) 229981

Contents lists available at ScienceDirect

Journal of Power Sources

journal homepage: www.elsevier.com/locate/jpowsour

A cost and time effective novel methodology to determine specific heat capacity of lithium-ion cells

Shrisha Balkur [a], Niladri Roy Chowdhury [a,*], Jens Groot [b], Torbjörn Thiringer [a]

[a] Department of Electrical Engineering, Division of Electric Power Engineering, Chalmers University of Technology, 412 96 Gothenburg, Sweden
[b] Volvo Group Trucks Technology (GTT), 405 08 Gothenburg, Sweden

HIGHLIGHTS

- Novel method to determine the specific heat capacity of lithium-ion cells.
- The method uses commonly available inexpensive equipment.
- The specific heat capacity of the cell can be obtained from a single experiment.
- The method is applicable to both prismatic and pouch cells.
- Results are validated using both calorimeter and thermal model.

GRAPHICAL ABSTRACT

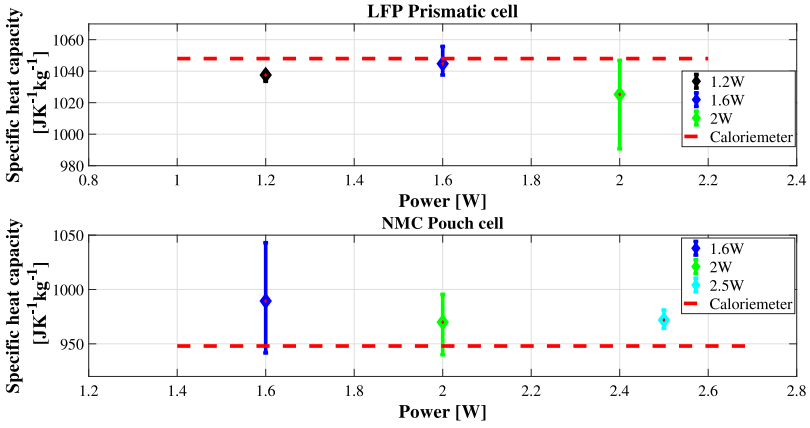

ARTICLE INFO

Keywords:
Lithium-ion cell
Specific heat capacity
Thermal modeling
Cost effective method
Time effective method

ABSTRACT

A cost and time-effective novel method for determining the specific heat capacity of prismatic and pouch lithium-ion cells using a simple setup and easily available equipment is presented in this paper. Specific heat capacity is an important thermal parameter of lithium-ion cells which is not readily available or provided by the cell manufacturers. The results found in this work are compared with the calorimetrically determined values of the specific heat capacity and a maximum error of 5% and 1.4% have been found for the pouch and the prismatic cells, respectively. The minimum error in the specific heat capacity for the pouch and the prismatic cells are 0.7% and 0.1%, respectively. The thermal parameters obtained using this methodology have been used to model the surface temperature of a prismatic cell during the application of a dynamic pulsed power as well as New European Driving Cycle (NEDC) and Worldwide harmonized Light vehicles Test Cycle (WLTC) drive cycles-based power traces. The excellent matching of the measured and simulated cell's surface temperature during both the NEDC and WLTC drive cycles demonstrates that the thermal parameters determined using this new method can be used to model the surface temperature of the cell.

1. Introduction

Electrochemical batteries are becoming a standard practice in applications like transportation, electronics and energy storage. Among all the other battery technologies as a power source for vehicle electrification lithium-ion battery (LIB) is the prime candidate. High power density, high specific energy, high theoretical capacity, long cycle-life

* Corresponding author.
E-mail address: niladri.roy.chowdhury@chalmers.se (N. Roy Chowdhury).

https://doi.org/10.1016/j.jpowsour.2021.229981
Received 28 February 2021; Received in revised form 7 April 2021; Accepted 29 April 2021
Available online 7 May 2021

and low self-discharge rate are some of the characteristics which make the LIB a proponent in the battery technology race [1,2].

The key parameters of LIB such as capacity, efficiency, internal resistance, lifetime and self-discharge are strongly influenced by the battery temperature. An undetected increase in battery temperature is a serious safety concern leading to overheating damage, thermal runaway and even fire. A suitable battery thermal management system can monitor and control the cell temperature within its optimal limits during its operation. Proper thermal modeling of LIBs is therefore required for the development of highly effective and robust on-board battery thermal management systems. Thermal modeling is vital for understanding the heat generation and heat transfer processes inside a cell. An important step in the thermal modeling of batteries is the development of a general energy balanced battery thermal model for estimating the heat generation rate of a single lithium ion cell by Bernardi et al. [3]. Various other thermal models have been proposed after that. These models can be broadly classified based on either physical mechanisms or on the order of their dimensional complexity. On the basis of physical mechanisms, thermal models can be classified as an electrochemical–thermal model [4–6], an electro-thermal model [7,8] and a thermal runaway model [9,10]. Based on the increasing order of dimension complexity the models can be categorized as a lumped-parameter model [11,12], a one-dimensional model [13], a two-dimensional model [14], a three-dimensional model [15,16] or a mixed-dimensional model [7].

All the above mentioned thermal models require heat capacity and thermal resistance of the cells as a model input. Depending on the level of complexity of the thermal model, either a single lumped value for the heat capacity of the entire cell or individual values for the heat capacity of the different layered materials of the cell is required. A frequently encountered problem is that neither information about the specific heat capacity nor the thermal resistance of a cell are readily available. There are several methods for experimentally determining the specific heat capacity of a cell. One of the methods is the semi-theoretical way to find the weighted sum of the heat capacities of the cell materials. This involves opening up a cell and then individually determining the specific heat capacity of the cell materials [17,18]. It is a very time-consuming process requiring special facilities and instruments that are not generally available in battery labs. The most common method today for measuring the specific heat capacity of a lithium-ion cell is the calorimetric method [19,20], but calorimeters are extremely expensive. On top of that, building and calibrating a new calorimeter is a time-consuming process [21]. Due to this, other than using calorimeters several different methods have been proposed in literature for determining the specific heat capacity of lithium ion cells [22]. An internal thermocouple installed inside a cell can be used to measure the specific heat capacity of the cell [23]. However, a temperature sensor can be installed inside a cell only inside a glovebox and there are substantial chances that the cell might be damaged during this process. Thermal impedance spectroscopy (TIS) is another method used to determine the specific heat capacity [24]. In the TIS method, current pulses at different frequencies are applied and the cell's surface temperature is measured. The cell's specific heat capacity is obtained from the Nyquist plot of the surface temperature. However, recording the battery thermal response, usually in the range of mHz is a very time consuming process and due to the variability of the cell's heat emission to the surrounding, an uncertain method. J. P. Schmidt introduced a new method called electrothermal impedance spectroscopy (ETIS) for measuring the thermal properties of lithium-ion cells [25,26] . In this method, a small frequency sinusoidal shaped heat excitation signal is applied to the cell and the cell's surface sinusoidal temperature is measured, then the cell's thermal impedance response is obtained. Thermal properties of the cell are obtained by fitting the thermal impedance to a thermal equivalent circuit. Similar to the TIS method this is also a very time consuming method and the unknown heat dissipation to the surrounding is a problem. Drake et al. have presented a simple method for measuring the an-isotropic thermal transport properties of a cell [27]. Their method is only limited to cylindrical cells and requires a vacuum chamber. A new and simple method for determining the heat capacity of lithium-ion cells has been proposed by Bryden et al. [28], however in their method they have used a battery cycler and their method requires two distinct tests, one with a fan and another without a fan to measure the specific heat capacity of the cell. In their method they have heated the cell internally by generating ohmic heat on applying current greater than 1C. At high currents there will be additional heat generation at the point of connection of the current carrying wires to the cell. These additional heat losses cannot be easily accounted for and can lead to uncertainties in the calculated values of the thermal parameters. Some researchers have used an external heat source to determine the specific heat capacity of cylindrical cells [17] by measuring the thermal parameters using special kinds of equipment. Recently, Murashko and co-workers have developed a simple and inexpensive method to simultaneously determine the specific heat capacity and through-plane thermal conductivity of any lithium-ion cylindrical cell by measuring the temperature and heat flux on the cell surface [29]. Zhang and co-workers have developed a new method to measure convective heat transfer coefficient and specific heat capacity of a lithium-ion battery using the lumped capacitance method [30]. However, their proposed method relies on using a relatively expensive infrared camera.

The purpose of this paper is to demonstrate a novel method for measuring the specific heat capacity of prismatic and pouch lithium ion cells. The method proposed in this paper is relatively simple and uses equipment commonly available in most battery laboratories. The proposed method does not use any special equipment like, vacuum chamber, calorimeter, glove box, temperature chamber, battery cycler or infrared camera. The thermal parameters of the cell can be determined in a single experiment thereby making it both a cost-effective and a time-effective method. The specific heat capacity of both the cells have been verified using the calorimetric method to prove the accuracy of this new method. The thermal parameters obtained for the prismatic cell has been used to model the surface temperature during application of dynamic heat pulses as well as NEDC and WLTC drive cycles to further validated the usefulness of this methodology. This new method will both reduce the cost and the time of thermal characterization of lithium-ion cells, without compromising the accuracy of the parameter identification. The specific heat capacity obtained using this method will help in developing thermal models and designing of the cooling systems for the LIB.

2. Electro-thermal analogy

In the proposed methodology, the Lumped Parameter Network (LPN) modeling approach for the parameter identification is used to extract the specific heat capacity of the cell. This paper uses the analogy between thermal and electrical phenomena as explained in Table 1 and more details can be found in books dealing with heat transfer [31]. Current sources represent the heat generation in the system, voltage sources represent the set temperature, while the voltages also represent the temperature at the nodes (associated with the lumped volumes). Thermal capacitance represents the heat stored in the nodes and thermal resistances represent the resistance to the transfer of heat by either conduction or convection between the nodes.

The basis of this analogy is the similarities between the electrical and the thermal equations. The first set of equations represent the charge stored in the capacitor due to the variation of current and the heat stored by the body with mass m having specific heat capacity C_p due to the variation of heat flux. This is given as

$$C\frac{dV(t)}{dt} = I(t) \tag{1}$$

$$mC_p\frac{dT(t)}{dt} = C_{th}\frac{dT(t)}{dt} = \dot{Q}(t). \tag{2}$$

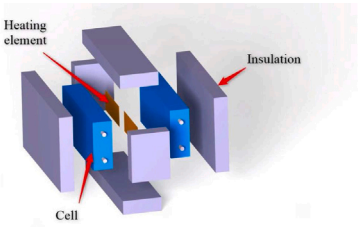

(a) Exploded view of the experimental setup.

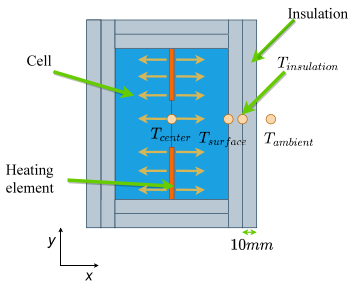

(b) Top view of the setup and the temperature sensors placement.

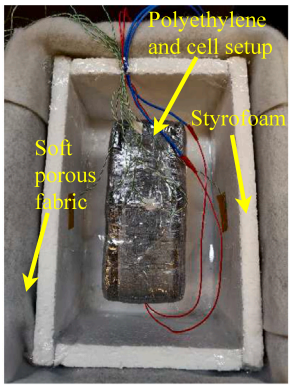

(c) Experimental setup of the cell and polyethylene placed in the Styrofoam box.

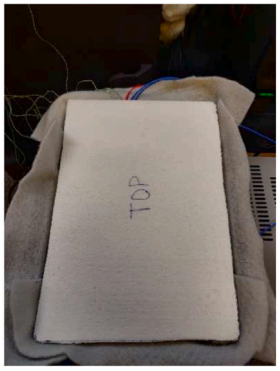

(d) The experimental setup with the Styrofoam lid.

Fig. 1. Experimental setup [32].

Table 1
Analogy between thermal and electrical parameters.

Thermal parameters	Electrical parameters
Temperature, T [K]	Voltage, V [V]
Heat flow, $\dot{Q}$ [W]	Current, I [A]
Thermal resistance, R_{th} [K W^{-1}]	Electrical resistance, R [Ω]
Thermal capacitance, C_{th} [J K^{-1}]	Electrical capacitance, C [F]

The second pair of analogous equations are Ohm's law and the one dimensional form of Fourier's law,

$$I(t) = \frac{1}{R}\Delta V(t) \tag{3}$$

$$\dot{Q}(t) = \frac{1}{R_{th}}\Delta T(t). \tag{4}$$

The thermal resistance R_{th} is dependent on both the heat transfer coefficients due to conduction h_{cond} and convection h_{conv}. It is given as

$$R_{th} = \begin{cases} \sum \frac{L}{h_{cond}A}, & \text{thermal resistance due to conduction} \\ \sum \frac{1}{h_{conv}A}, & \text{thermal resistance due to convection} \end{cases} \tag{5}$$

where, L [m] and A [m^2] are the thickness and the cross section area of the body, respectively. Eqs. (1)–(4) show the similarity between the electrical and thermal parameters and hence the heat transfer can be modeled using electrical networks. The procedure to build the thermal network has been previously discussed in [33] and this method will be used in the further analysis.

3. Experimental setup

Detailed description of the experimental setup for the new methodology to extract the thermal parameters of a lithium-ion cell is discussed in this section. As discussed earlier the main advantage of the method described in this paper is that it requires simple and easily available equipment for thermal characterization of a cell. The setup consists of: two identical cells which need to be characterized, Kapton insulated flexible heaters, insulating material with known specific heat capacity, at least four temperature sensors and finally a power supply to power the flexible heater. In addition to being cheap and simple, using this method both the specific heat capacity and the internal thermal resistance of a cell can be obtained by performing a single test, thereby making it a time-effective method. In this paper the internal thermal resistance of the cell has been approximated to a single value in the through-plane (across the stack layers) direction. The flexible heaters are sandwiched between the two identical cells and an insulating material is used to cover the setup from all sides as shown in Fig. 1(a).

The use of insulating material to cover the cells helps in a better entrapment of heat. The insulating material makes the representation of the setup a second order thermal model, which makes it possible to extract both the thermal parameters from a single test using the equation developed in Section 4. In principle, any insulation material with known specific heat capacity can be used for the setup. In this work, polyethylene foam having a measured volumetric mass density, $\rho = 29.5\,\text{kg m}^{-3}$ and thickness of 10 mm is used as an insulating material. The specific heat capacity of the insulation material according to [34] is 2450.7 J K^{-1} kg^{-1} for polymer's density in the range of 16.7 kgm^{-3} to 69.5 kg m^{-3}. This value of the specific heat capacity of the insulation material is used in further calculations. Kapton insulated flexible

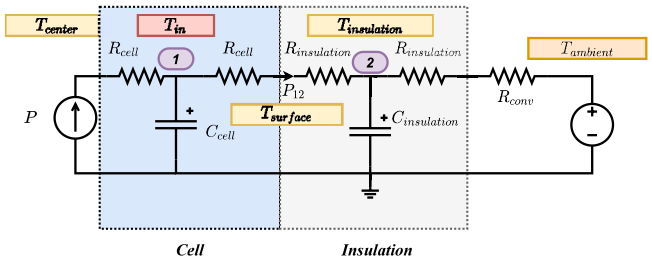

Fig. 2. Thermal circuit of the experimental setup [32].

heaters are used as the heating element. The 0.254 mm thickness of the heater is useful in this particular application as it minimizes the air gap thereby establishing a good thermal contact between the two cells. Thermal copper paste is also applied to improve the thermal contact between the two cells. Four K-type temperature sensors are used to record the temperature at a sampling frequency of 1 Hz. The placement of the temperature sensors in the setup can be seen in Fig. 1(b).

The first sensor is placed at the center in between the two cells, the second one on the surface between the cell and the insulation material, the third one between the two layers of insulation material and finally the last temperature sensor measures the ambient temperature. The whole setup is placed inside a thermally insulated box to avoid fluctuations in the external temperature variations during the test as shown in Fig. 1(c).

The whole setup is then placed inside a plastic box covered completely from the inside by a soft porous insulating fabric. In addition to that, styrofoam sheets are used to cover all the five surfaces of the box from inside to minimize the heat loss. Finally the box is closed from the top using a styrofoam sheet lid. An EL302RT power supply is used to supply known power to the heaters for heating up the setup.

4. Theoretical model

The basic lithium-ion cell thermal model previously discussed in the literature is the basis of this new methodology [23,28]. In this thermal model, heat is generated at one of the surfaces of the cell using a flexible heater. The generated heat is then transferred through the cell to the opposite surface. The cell surface is considered to have no mass and as a consequence no specific heat capacity. Finally, the heat is transferred from the surface of the cell to the surroundings through the insulation layer. Mass and specific heat capacities of the cell and the insulation are lumped together to points at the center of their respective volumes. The thermal circuit of the setup for one cell is shown in Fig. 2.

In Fig. 2 T_{center} is the temperature at the surface of the cell where the heat is generated, T_{in} is the internal temperature of the cell, $T_{surface}$ is the temperature of the cell surface between the cell and the insulation material, $T_{insulation}$ is the temperature at the center of the insulating material and $T_{ambient}$ is the ambient temperature. R_{cell} is the internal thermal resistance of the cell in the through-plane direction, $R_{insulation}$ is the thermal resistance across the single insulating material layer and R_{conv} is the convective thermal resistance from the surface of the insulating material to the ambient temperature sensor. Here R_{cell} represents the conductive thermal resistance from the center of the cell to the cell surface with larger area. If $R_{cell,total}$ is the total thermal resistance of the cell between T_{center} and $T_{surface}$, then R_{cell} is half of the total thermal resistance of the cell,

$$R_{cell} = \frac{R_{cell,total}}{2}. \tag{6}$$

C_{cell} and $C_{insulation}$ are the heat capacities of the cell and the insulating material, respectively. **1** and **2** are the two nodes in the thermal circuit. As the experimental setup is symmetric in nature the other cell also has the same thermal network as shown in Fig. 2. Due to the symmetric nature of the experimental setup, the distribution of the rate of change of heat ($\dot{Q}$) is assumed to be equal in both the directions of the Kapton insulated flexible heater. The power supplied to one cell (P) can be expressed as

$$P = \dot{Q} = \frac{P_W}{2} \tag{7}$$

where P_W is the power supplied to the heater. It is difficult to place a temperature sensor at the center of an insulating material layer to measure $T_{insulation}$. This problem is overcome by considering two identical layers of the insulating material as a single unit and $T_{insulation}$ is measured in between these two layers. $C_{insulation}$ ($\mathrm{J\,K^{-1}}$) is the product of specific heat capacity of the insulating material and the combined mass of both the layers.

On the basis of the direction of heat flow one can express the heat balance equation at node **1** as

$$P = C_{cell}\frac{dT_{in}(t)}{dt} + \frac{T_{in}(t) - T_{insulation}(t)}{R_{in}} \tag{8}$$

where the rate of heat generated (P) by the heater at the surface of the cell is equal to the sum of the heat stored at this node due to the heat capacity of the cell, and the rate that the heat flows away from this node. The rate of the heat stored at node **1** is related to the product of change in T_{in} with respect to time and C_{cell}.

The rate with which heat flows away from node **1** is related to the heat transfer coefficient of the cell and the temperature difference between T_{in} and $T_{surface}$. Since there is no mass at the interface between the surface and the insulation, there is no heat storage at this interface and the same heat flows towards **2** due to the thermal conductivity of the insulation and the temperature difference between $T_{surface}$ and $T_{insulation}$. Therefore, the heat transfer from **1** to **2** can be represented as the temperature difference between T_{in} and $T_{insulation}$ divided by the thermal resistance between these two nodes R_{in}. R_{in} can be expressed as a sum R_{cell} and $R_{insulation}$

$$R_{in} = R_{cell} + R_{insulation}. \tag{9}$$

Similarly, the heat balance at node **2** can be expressed as

$$\frac{T_{surface}(t) - T_{insulation}(t)}{R_{insulation}} = C_{insulation}\frac{dT_{insulation}(t)}{dt} + \frac{T_{insulation}(t) - T_{ambient}}{R_{out}}. \tag{10}$$

The term on the left hand side of Eq. (10) represents the rate of heat transfer to node **2**. The right hand side of Eq. (10) represents the rate at which heat is stored at this node and the rate at which heat flows out from this node. The rate at which heat is transferred to node **2** depends on the temperature difference between $T_{surface}$, $T_{insulation}$ and the inverse of $R_{insulation}$. The rate at which heat is stored at this node is dependent on the product of $C_{insulation}$ and change in $T_{insulation}$ with respect to time. On the other hand, the rate at which heat is transferred away from this node is related to the temperature difference between the $T_{insulation}$ and $T_{ambient}$ and inverse of R_{out}. R_{out} can be expressed as the sum of $R_{insulation}$ and R_{conv}

$$R_{out} = R_{conv} + R_{insulation}. \tag{11}$$

The heat balance equation at node **1** described in Eq. (8) relies on the measurement of T_{in}, which is not an easily measurable quantity. Measuring the T_{in} requires placement of a thermocouple inside the cell. Placing a thermocouple inside a cell requires an inert atmosphere so that the components of the cell are not damaged by the oxygen and the moisture in the air when inserting the thermocouple. An inert atmosphere requires a glove box which is not readily available in all laboratories. The need for measuring the internal temperature of the cell can be eliminated by considering the fact that the same heat flows

between node **1** and node **2**. So the flow of heat between the nodes, P_{12} can be represented as

$$P_{12} = \frac{T_{in}(t) - T_{surface}(t)}{R_{cell}} = \frac{T_{surface}(t) - T_{insulation}(t)}{R_{insulation}} = \frac{T_{in}(t) - T_{insulation}(t)}{R_{in}}. \tag{12}$$

Under the consideration that the same heat flows between node **1** and node **2** the heat balance equation at node **2** described in Eq. (10) can be modified as

$$\frac{T_{in}(t) - T_{insulation}(t)}{R_{in}} = C_{insulation}\frac{dT_{insulation}(t)}{dt} + \frac{T_{insulation}(t) - T_{ambient}}{R_{out}}. \tag{13}$$

Rearranging Eq. (13) we get

$$T_{in}(t) = R_{in} \times \left(C_{insulation}\frac{dT_{insulation}(t)}{dt} + \frac{T_{insulation}(t) - T_{ambient}}{R_{out}} + \frac{T_{insulation}(t)}{R_{in}}\right). \tag{14}$$

A second order differential equation in terms of $T_{insulation}$ is obtained by replacing T_{in} from Eq. (14) in Eq. (8) as

$$T_{insulation}(t) = PR_{out} + T_{ambient} - \alpha\left(\frac{dT_{insulation}(t)}{dt}\right) - \beta\left(\frac{d^2T_{insulation}(t)}{dt^2}\right) \tag{15}$$

where

$$\alpha = C_{cell}R_{in} + C_{cell}R_{out} + C_{insulation}R_{out} \tag{16}$$

and

$$\beta = C_{cell}R_{in}C_{insulation}R_{out}. \tag{17}$$

The second-order differential equation is solved by the Laplace transform method using two initial conditions, $T_{insulation}(t = 0) = T_{ambient}$ and $\frac{dT_{insulation}(t=0)}{dt} = 0$. Using the Laplace transform method and the two initial conditions, $T_{insulation}$ in the Laplace domain can be expressed as

$$T_{insulation}(s) = \frac{\beta s + \alpha T_{ambient} + \frac{T_{ambient}}{s} + \frac{PR_{out}}{s}}{\beta s^2 + \alpha s + 1} \tag{18}$$

where s is the Laplace transform variable for time (t). $T_{insulation}$ in time domain is obtained by taking the inverse Laplace transform of Eq. (18) and is expressed as

$$T_{insulation}(t) = T_{ambient} + PR_{out}\left[1 - \exp\left(\frac{-\zeta t}{\tau}\right)\left(\cosh\left(\frac{t\sqrt{\zeta^2-1}}{\tau}\right) - \frac{\zeta}{\sqrt{\zeta^2-1}}\sinh\left(\frac{t\sqrt{\zeta^2-1}}{\tau}\right)\right)\right] \tag{19}$$

where

$$\tau = \sqrt{\beta} = \sqrt{C_{cell}R_{in}C_{insulation}R_{out}} \tag{20}$$

and

$$\zeta = \frac{\alpha}{2\sqrt{\beta}} = \frac{C_{cell}R_{in} + C_{cell}R_{out} + C_{insulation}R_{out}}{2\sqrt{C_{cell}R_{in}C_{insulation}R_{out}}}. \tag{21}$$

Eq. (19) is similar to the general solution of a second order over-damped equation. A system is considered to be over-damped if the response to a step input slowly moves towards steady state without oscillations. $T_{insulation}$ on applying an input heat step slowly reaches steady state without any oscillation. ζ and τ are the damping coefficient and time constant of the system, respectively. ζ and τ are both system parameters, the former describes how oscillations in a system decay after applying an input, the latter represents the elapsed time required for the system response to reach steady state if the system had continued to grow at the initial rate. For an over-damped system ζ is > 1. In the next section it will be discussed, using Eq. (19), how the parameters of interest, i.e. specific heat capacity and thermal resistance of a cell can be obtained.

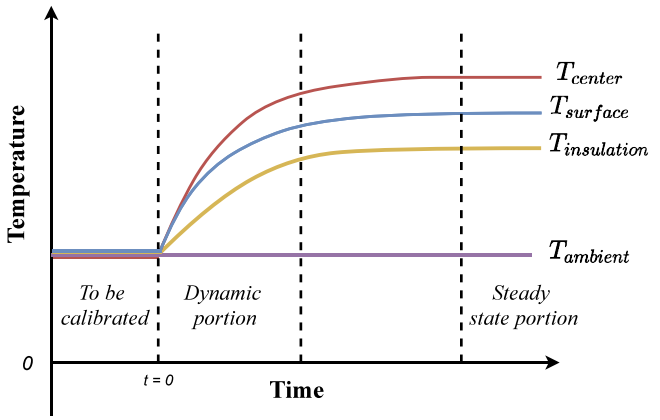

Fig. 3. Test for finding $C_{P_{cell}}$ and R_{cell}.

5. Parameter extraction

In this section, first the testing procedure is briefly explained, before discussing about the parameter extraction process. The experimental setup described in Section 3 is used for conducting the experiments. At the beginning of each experiment no power is applied to the setup for a minimum duration of ten minutes. A constant ambient temperature is maintained during the entire duration of the experiments. A specified power is applied to the flexible heater which heats up the setup. The test is continued until all the temperatures reach a steady state. The minimum power applied to the heater is selected such that the difference between $T_{ambient}$ and T_{center} at steady state is at least 10 °C. The maximum applied power is chosen such that the cell temperature does not exceed the recommended safety limit.

Discussion about the parameter extraction process can be divided into two sections. In the first section, determination of the thermal resistances will be discussed. In the final section, calculation of the specific heat capacity will be performed. Two significant portions of the experimental data are identified, namely the dynamic and the steady state portion as can be seen in Fig. 3. Usually in the initial portion, the temperature sensors have offset errors which affect the results. Using the temperature data from the initial period the temperature sensors are calibrated so that they have the same value during that period.

All the thermal resistances present in the thermal circuit as shown in Fig. 2 are calculated based on the data from the steady-state portion of the plots and discussed in Section 5.1. The heat capacity of the cell is calculated in Section 5.2 using the dynamic portion of the $T_{insulation}$ plot.

5.1. Thermal resistances

The steady state segment of the temperature vs time plots are used for calculating all the thermal resistances of the thermal model. At steady state all the temperatures, namely T_{center}, $T_{surface}$ and $T_{insulation}$ remain constant, as a result we have

$$\frac{dT_{center}}{dt} = \frac{dT_{surface}}{dt} = \frac{dT_{insulation}}{dt} = 0. \tag{22}$$

The system is not influenced by either C_{cell} or $C_{insulation}$ at steady state. The same heat flows through each thermal resistances in the thermal circuit at steady state. The average values of the temperatures

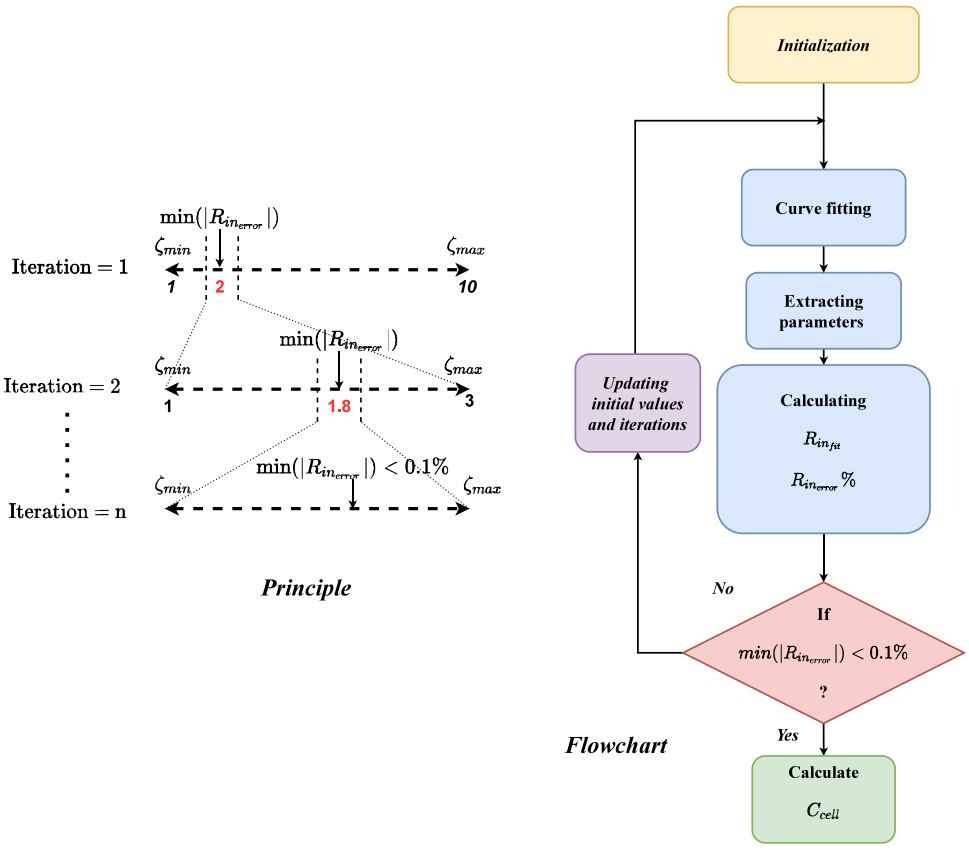

Fig. 4. Algorithm to select the correct value of ζ for calculating C_{cell}.

in the final segment are considered when calculating the thermal resistances. R_{cell} is calculated using the difference between the average value of both T_{center} and $T_{surface}$ at steady state and then dividing it by P

$$R_{cell} = \frac{\bar{T}_{center}(t=\infty) - \bar{T}_{surface}(t=\infty)}{2P} \tag{23}$$

where $\bar{T}$ denotes the average value of a particular temperature. The factor of 2 in the denominator of Eq. (23) accounts for the presence of two R_{cell} between the points where T_{center} and $T_{surface}$ are measured. Similarly, $R_{insulation}$ is obtained as

$$R_{insulation} = \frac{\bar{T}_{surface}(t=\infty) - \bar{T}_{insulation}(t=\infty)}{P}. \tag{24}$$

At steady state, Eq. (15) can be simplified to Eq. (25) from which R_{out} can be calculated

$$R_{out} = \frac{\bar{T}_{insulation}(t=\infty) - \bar{T}_{ambient}(t=\infty)}{P}. \tag{25}$$

Using Eq. (11) R_{conv} can be calculated from the difference between R_{out} and $R_{insulation}$ as

$$R_{conv} = R_{out} - R_{insulation}. \tag{26}$$

5.2. Specific heat capacity

The heat capacity of the cell is obtained by performing curve fitting on the dynamic portion of the insulation temperature data using Eq. (19). Curve fitting is done with the help of the Matlab curve fitting toolbox [35]. The robust non-linear least square method is used for fitting the curve. τ and ζ are extracted using the curve fitting. The physically significant value of C_{cell} can be obtained only if the correct upper and lower limits of the ζ are selected. An algorithm for selecting the right values of the lower (ζ_{min}) and the upper (ζ_{max}) limits of ζ is proposed. The main principle of this algorithm for selecting ζ_{min} and ζ_{max} is to minimize (<0.1%) the absolute error between R_{in} and $R_{in_{fit}}$. $R_{in_{fit}}$ is the value of the internal thermal resistance obtained from curve fitting Eq. (19) and R_{in} is the sum of R_{cell} and $R_{insulation}$ calculated using Eq. (23) and Eq. (24), respectively.

A parameter sweep for ζ is performed in an interval between ζ_{min} and ζ_{max} with a fixed step size m. During the first iteration $m = 1$ is selected as the step size. Curve fitting for the initial section of the $T_{insulation}(t)$ curve is done to extract the fitted values of the time constant, τ_{fit} and the damping coefficient ζ_{fit}. τ_{fit} is the square root of the product of the fitted internal ($\tau_{in_{fit}}$) time constant and the external (τ_{out}) time constant

$$\tau_{fit} = \sqrt{\tau_{in_{fit}} \times \tau_{out}}. \tag{27}$$

The external (τ_{out}) time constant is the product of $C_{insulation}$, which is a known quantity and the experimentally measured R_{out}

$$\tau_{out} = C_{insulation} R_{out}. \tag{28}$$

The fitted internal ($\tau_{in_{fit}}$) time constant is the product of the fitted heat capacity of the cell $C_{cell_{fit}}$ and the internal thermal resistance $R_{in_{fit}}$

$$\tau_{in_{fit}} = C_{cell_{fit}} R_{in_{fit}} = \frac{\tau_{fit}^2}{\tau_{out}}. \tag{29}$$

Using Eq. (21) and Eq. (20) $C_{cell_{fit}}$ is calculated as

$$C_{cell_{fit}} = \frac{2\tau_{fit}\zeta_{fit} - \tau_{out} - \tau_{in_{fit}}}{R_{out}}. \tag{30}$$

Once the value of $C_{cell_{fit}}$ is known, then $R_{in_{fit}}$ can be calculated from Eq. (29) as

$$R_{in_{fit}} = \frac{\tau_{in_{fit}}}{C_{cell_{fit}}}. \tag{31}$$

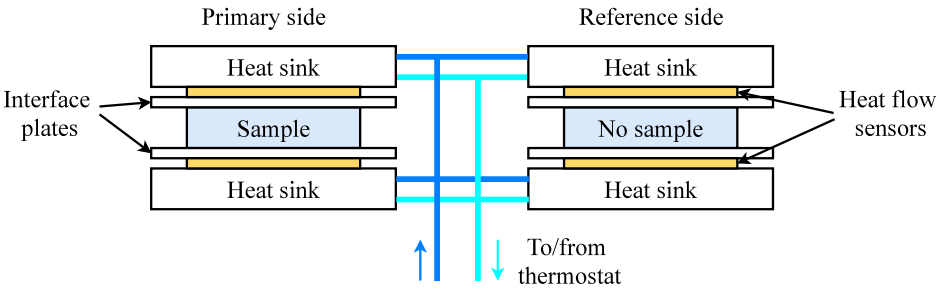

(a) Overview of calorimeter.

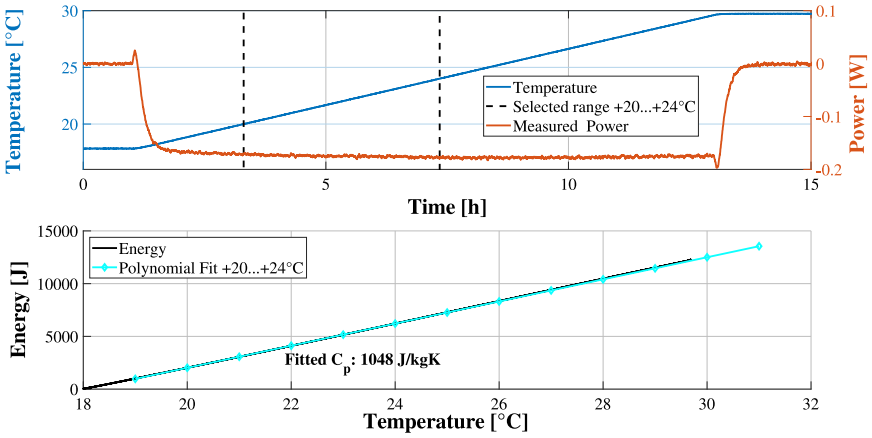

(b) Upper figure: Measured sample temperature and calorimeter heat flow [W] during constant heating test used to measure heat capacity. Lower figure: calculated energy vs. sample temperature and fitted $\mathrm{d}W/\mathrm{d}T = C_p$.

Fig. 5. Calorimeter overview and test results.

The percentage error between the experimentally obtained value of R_{in} and its fitted value $R_{in_{fit}}$ is calculated as

$$R_{in_{error}} = \frac{R_{in} - R_{in_{fit}}}{R_{in}} \times 100. \tag{32}$$

After the first iteration, if the absolute value of $R_{in_{error}}$ is greater than 0.1 % then the same procedure is repeated after updating the values of ζ_{max} and ζ_{min}. In order to update the values ζ_{max} and ζ_{min}, from the previous parametric sweep of ζ, the particular index of ζ_N is selected for which $R_{in_{error}}$ is minimum in that given parametric sweep. The new values of ζ_{max} and ζ_{min} are selected for the next iteration as

$$\left.\begin{aligned}\zeta_{min} &= \zeta_N - m \\ \zeta_{max} &= \zeta_N + m\end{aligned}\right\} \text{Where, } m = 0.1^{iter-1} \quad \forall iter = 1, 2, 3, \ldots, n \tag{33}$$

$iter$ is the iteration number ranging from 1 to n. The next iteration is run with these newly updated values of ζ_{max} and ζ_{min} and the updated step size m is reduced by a factor of 10. This process is repeated until the absolute value of $R_{in_{error}}$ is less than 0.1 %. The values of ζ and τ corresponding to this least value of $R_{in_{error}}$ are used to calculate C_{cell} [J K^{-1}] from Eq. (30). The specific heat capacity of the cell is calculated $C_{p_{cell}}$ [Jkg^{-1}K^{-1}] after dividing the heat capacity of the cell C_{cell} by the weight of the cell m_{cell}

$$C_{p_{cell}} = \frac{C_{cell}}{m_{cell}}. \tag{34}$$

The above mentioned algorithm is explained graphically in Fig. 4.

6. Calorimetric measurements

A custom-made cell calorimeter (Fig. 5(a)) was used to validate the presented characterization method. The calorimeter is an isothermal conduction calorimeter based on a measurement of heat flow through thermopiles mounted between heatsinks and interface plates, in turn in contact with the sample cell. A liquid circulator-thermostat circulates water at a very precise temperature (±0.01 °C) through the heat sinks, effectively maintaining isothermal conditions. Since the thermopiles and the interface plates provide a path with very high thermal conductivity between sample cell and the heat sinks, any heat produced or absorbed by the sample cell will flow through the thermopile sensors, in turn producing a voltage signal in the millivolt range that is linearly correlated to the heat flow. A differential setup of two identical calorimeters, in Fig. 5(a) labeled as “Primary” and “Reference”, is used to further reduce measurement noise and increase the practical sensitivity. Here, the primary side carries the sample and the reference is empty, hence providing a baseline for the measurement equally affected by slight variations in temperature from the thermostat or leakage to ambient air. That is, all calculations are based on the differential signal primary-reference rather than relying on a direct measurement from the side carrying the sample. To further increase the accuracy, both primary and reference calorimeter were placed side by side inside a thermally insulated box to reduce influence of fluctuations in ambient air (±1 °C). A complete description of the calorimeter is given elsewhere [21,36].

Although the calorimeter is isothermal, measurement of a sample’s specific heat capacity can be done by either applying a step-wise

Table 2
Cell and insulation material details.

Parameter	LFP prismatic	NMC pouch
Cell specifications		
Manufacturer	GWL-power	LG
Geometry	Prismatic	Pouch
Chemistry	LFP/C	NMC/C
Capacity	20 A h	37 A h
Weight	0.61 kg	0.56 kg
Dimensions	178 mm × 71 mm × 28 mm	232 mm × 164 mm × 8 mm
Maximum voltage	3.65 V	4.2 V
Minimum voltage	2.8 V	2.5 V
Insulation material details		
Density	$29.5\ kgm^{-3}$	
Dimensions	210 mm × 110 mm × 20 mm	295 mm × 204 mm × 20 mm
$C_{insulation}$	$33.37\ J\ K^{-1}$	$86.99\ J\ K^{-1}$

Table 3
Parameters calculated for the tests done at different applied power for the LFP prismatic cell. All the thermal resistances in the table have an unit of KW^{-1}, the time constant τ has an unit of s and ζ is a dimensionless parameter.

Parameters	Power applied	Trial 1	Trial 2	Trial 3
R_{cell}	1.2 W	0.76	0.76	0.76
$R_{insulation}$		6.37	6.48	6.40
R_{conv}		10.45	10.49	10.86
τ		1588.30	1603.30	1612.60
ζ		4.93	4.90	4.95
$C_{p_{cell}}$		1039.80	1033.60	1039.30
R_{cell}	1.6 W	0.74	0.74	0.76
$R_{insulation}$		6.42	6.42	6.39
R_{conv}		9.49	10.70	10.99
τ		1560.70	1607.10	1615.40
ζ		4.90	4.94	4.54
$C_{p_{cell}}$		1055.70	1040.90	1037.60
R_{cell}	2.0 W	0.75	0.75	0.76
$R_{insulation}$		6.34	6.30	6.53
R_{conv}		10.49	10.49	10.96
τ		1583.80	1583.70	1265.90
ζ		4.93	4.95	4.47
$C_{p_{cell}}$		1038.30	1049.80	990.74[a]

[a]Experiment done without lid.

change in temperature within a relatively narrow range ($\Delta T < 5$ °C) and carefully integrating the corresponding heat flow to/from the sample, or by applying a constant heating/cooling rate (constant dT/dt) and determining the average steady-state heat flow. In the present work the second method was applied in a relatively narrow temperature range, see Fig. 5(b). Several tests, with different temperature windows and temperature ramps, were carried out in order to find an adequate compromise between signal to noise ratio and quasi-isothermal conditions where the sample temperature was kept very close to that of the heat sink, indicating uniform sample temperature and semi-equilibrium conditions. Finally, a positive temperature ramp at +1 °C per hour was applied to the sample.

As can be seen in Fig. 5(b) showing the measurements on the prismatic 20Ah LFP cell (Table 2), the measured heat-flow is close to constant with respect to temperature although the slight increase at higher temperatures indicate a loss of heat to ambient air, despite the thermally insulated and differential setup. Hence, the calculation of specific heat capacity is performed using measurement of heat flow in a narrow range centered around the ambient air temperature: +20...+24 °C. Still, the fitted value (lower part of Fig. 5(b)) corresponds relatively well to the entire temperature range of +18...+30 °C.

7. Results and discussions

The new method is used to determine specific heat capacity of two lithium-ion cells of different chemistries and formats. Details of the two cells are given in Table 2. The exact chemistries of the cells are unknown but the prismatic cell uses Lithium Iron Phosphate (LPF) as the cathode material whereas the pouch cell uses Nickel Manganese Cobalt (NMC) as the cathode material. The data sheets for both the cells have no information about the specific heat capacity.

In this section, the experimental results for the prismatic cell will be discussed first followed by the pouch cell results. This section then proceeds into the validation test results to demonstrate that the thermal parameters obtained using this methodology can effectively model the temperature of a cell under various scenarios.

7.1. Thermal parameters

The power levels used for heating the prismatic cell are P_W = 1.2 W, 1.6 W and 2 W. All the experiments for the prismatic cell are done with the styrofoam lid to cover the top. A single experiment for the 2 W power level has been done without the styrofoam lid on the top to demonstrate how the variation in the external temperature can influence the experimental result. The experimental results of the LFP prismatic cell for the three different powers are tabulated in Table 3.

Table 4
Error tabulation of the calculated values in comparison to the Calorimetric value for the LFP prismatic cell.

Calorimeter $C_{p_{cell}}$ [J kg^{-1} K^{-1}]	Power applied [W]	$C_{p_{cell}}$ calculated [J kg^{-1} K^{-1}]	Error [%]	Average Error [%]
1048	1.2	1039.80	0.78	1.00
		1033.60	1.40	
		1039.30	0.83	
	1.6	1055.70	−0.73	0.31
		1040.90	0.68	
		1037.60	0.99	
	2.0	1038.30	0.93	0.51[b]
		1046.80	0.10	
		990.74[a]	5.46	

[a]Experiment done without lid.
[b]Excluding the without lid experimental result.

The values of the parameters in the table above give a clear indication that for a given condition, the system parameters, namely R_{cell}, $R_{insulation}$, R_{conv}, τ and ζ remain constant without a significant variation and are independent of the applied power. The minor variation in their values are due to the change in $T_{ambient}$ which has changed maximum 1 °C during the course of the experiment. Among all the experimental trials the one without the lid shows maximum variation in the system parameters, as the system is losing heat to the surroundings at a faster rate in this case, thereby reaching the steady state earlier compared to the other cases resulting in a lower value of the time constant τ. For each cell, three experiments at a given power has been conducted, giving a total of nine calculated values of $C_{p_{cell}}$ for each cell. The values of $C_{p_{cell}}$ of the prismatic cell for the three different applied power and their variations with respect to the calorimetrically calculated value are tabulated in Table 4. Table 4 also shows the error in the calculated value of $C_{p_{cell}}$ for the different applied power levels using the new method and the calorimetrically calculated value. From Table 4 it is clear that we get a maximum error of 5.46% for the experiment where the setup in the box has not been covered with the lid. In the uncovered setup the temperature readings for $T_{insulation}$, T_{core} and $T_{surface}$ get effected by the variation in the external temperature as $T_{ambient}$ has changed more than 1 °C during the course of the experiment. The average error in the calculated values of $C_{p_{cell}}$ in comparison to the calorimetric value for the prismatic cell are tabulated in Table 4.

From Table 4 we can see that the average error for the 1.2 W experiment is 1%, for the 1.6 W experiment the average error is 0.31% and for the 2 W experiment the average error is 0.51%. The results suggest that the calculated thermal parameters from this new methodology are independent of the applied power. The analysis of the results for the prismatic cell suggests that if the influence of the variation in the external temperature can be eliminated, then only one test at any specified power is sufficient enough to get $C_{p_{cell}}$ and the calculated value of $C_{p_{cell}}$ can be expected to have an error of less than 2%. Next we are going to discuss the results from the pouch cell.

In the case of the pouch cell, similar to the prismatic cell three different power levels have been selected and for each power three experiments are conducted. The applied power levels selected for the pouch cell experiment are 1.6 W, 2 W and 2.5 W. The experimental results for the pouch cell are tabulated in Table 5.

The results from Table 5 indicate that the system parameters namely R_{cell}, $R_{insulation}$, R_{conv}, τ and ζ do not vary significantly with the applied power levels. The minor differences in the values of the system parameters are due to the slight change in the ambient conditions. The experimental setup has been disturbed during trial 1 for the 1.6 W test to demonstrate how it can result in wrongly calculated value of $C_{p_{cell}}$. This disturbed experimental result is discussed in detailed in the supplementary data.

Table 6 shows the variation in the calculated values of $C_{p_{cell}}$ for the pouch cell with respect to the calorimetrically calculated value for different applied power levels. The percentage error between the calculated and calorimetric value for $C_{p_{cell}}$ of the pouch cell for different applied power are also tabulated in Table 6.

From Table 6 it can be seen that the average percentage error for 1.6 W, 2 W and 2.5 W powers are −1.52%, −2.3% and −2.52%, respectively. The percentage error in $C_{p_{cell}}$ values for the pouch cell is higher than for that of the prismatic cell. This model uses only one temperature sensor at the surface of the cell to calculate the $C_{p_{cell}}$ and does not take into account the variation of temperature across the surface of the cells. Thus, the reason for the higher error in the case of pouch cell is that it has a polymeric casing while the prismatic cell has an aluminum metal casing due to which it is possible to get uniform surface heating in the case of prismatic cell thereby giving better results. The results when compared with the calorimetric values indicates that neglecting the variation in temperature across the cell surface is not a major issue and can be considered as a valid assumption.

The specific heat capacities obtained using this new methodology matches closely with the calorimetric results. Neglecting the experimental case without lid the absolute maximum and the absolute minimum percentage error in the calculated value of the $C_{p_{cell}}$ for the prismatic cell are 1.40% and 0.10%, respectively. For the pouch cell the absolute maximum and the absolute minimum percentage error in the $C_{p_{cell}}$ are -5% and 0.70%, respectively if we exclude the disturbed experimental setup result. We can conclude from these results that only one experiment at any specified power can give a satisfactory value of $C_{p_{cell}}$. In this paper it has been assumed that the cell has a single value of the thermal resistance in the through-plane direction. This simple assumption accounts for the heat conducted only in one direction. The thermal resistance obtained using this method gives an indicative value of the internal thermal resistance of the cell. In the next sub-section we are going to discuss about validation tests to prove that the thermal parameters of the cell obtained from this new methodology can be used for modeling the temperature of the cell under various scenarios.

7.2. Validation tests

The cell thermal parameters obtained using this new method has been used to model the surface temperature of the cell under the applied dynamic power profile to test the validation of this method. Two distinct validation tests have been done, in the first validation test, external dynamic power pulses are applied to the cell and the surface temperature of the cell is recorded. In the second validation test the cell is heated internally by applying current from WLTC and NEDC drive cycles and the cell's surface temperature is recorded. For the validation purpose, only the LFP prismatic cell is used since electro-thermal model for the LFP prismatic cell has been previously developed in [32] and both reversible and irreversible losses can be calculated using this model. A first order thermal model is used for the validation purpose. In order to make the system a first order thermal model, one of the outer insulation layer on the surface of the cell is removed as shown in Fig. 6(a).

Table 5
Parameters calculated for the tests done at different applied power for the NMC pouch cell. All the thermal resistances in the table have an unit of KW^{-1}, the time constant τ has an unit of s and ζ is a dimensionless parameter.

Parameters	Power applied	Trial 1	Trial 2	Trial 3
R_{cell}	1.6 W	0.20	0.18	0.20
$R_{insulation}$		4.39	4.38	4.40
R_{conv}		3.70	3.70	3.62
τ		1374.60	1167.40	1197.40
ζ		2.95	3.10	3.15
$C_{p_{cell}}$		1043.00[a]	941.70	983.50
R_{cell}	2.0 W	0.18	0.20	0.20
$R_{insulation}$		4.31	4.31	4.37
R_{conv}		4.00	3.60	3.73
τ		1196.20	1150.30	1204.20
ζ		3.16	3.10	3.17
$C_{p_{cell}}$		974.20	940	995.50
R_{cell}	2.5 W	0.20	0.19	0.18
$R_{insulation}$		4.27	4.26	4.34
R_{conv}		3.70	3.70	3.40
τ		1167.90	1160.60	1162.60
ζ		3.14	3.13	3.13
$C_{p_{cell}}$		970.22	964.35	981.10

[a]Disturbed experimental setup.

Table 6
Error tabulation of the calculated values in comparison to the calorimetric value for the NMC pouch cell.

Calorimeter $C_{p_{cell}}$ [$J kg^{-1} K^{-1}$]	Power applied [W]	$C_{p_{cell}}$ calculated [$J kg^{-1} K^{-1}$]	Error [%]	Average Error [%]
948	1.6	1043.00[a]	−10.00	−1.52[b]
		941.67	0.70	
		983.50	−3.74	
	2	974.23	−2.77	−2.31
		940.00	0.84	
		995.50	−5.00	
	2.5	970.22	−2.34	−2.52
		964.35	−1.72	
		981.00	−3.50	

[a]Disturbed experimental setup.
[b]Excluding the disturbed experimental result.

Three temperature sensors are used to measure the temperatures at the center between the two cells, at the surface of the cell and the ambient temperature. The first step for the validation test is to determine the external thermal resistance, R_{out} (discussed in the supplementary data). After finding R_{out} from the first test, the validation test is performed. In the validation test a pulse power profile is applied to the cell and the surface temperature of the cell is recorded. 0.75 W of power is applied to a single cell for two hours followed by one hour of rest, this process is repeated three times. A Simscape first order thermal model is used to model the variation in the surface temperature on applying the dynamic pulse power. The Simscape model shown is Fig. 6(b) has two inputs, namely, P and $T_{ambient}$. $T_{surface}$ is the output. The calculated values of $C_{P_{cell}}$, R_{cell} and R_{out} are fed to the Simscape model. The result of the validation test is shown in Fig. 6(c). The average value of $C_{P_{cell}}$ and the R_{cell} for the 2 W power experimental test is used for the simulation shown in Fig. 6(c).

The measured (blue curve) and the simulated (red curve) surface temperatures are showing excellent match as evident from Fig. 6(c). The error between the experimental and the simulated temperature measurements for average values of $C_{P_{cell}}$ and R_{cell} for the three different power levels are tabulated in Table 7. The maximum error between the model and the experiment for all the trials is within 0.42 °C. The RMS error is lesser than 0.12 °C. This indicates that the values of $C_{P_{cell}}$ and R_{cell} of the cell are reasonable.

Next, the thermal parameters are validated with the WLTC and NEDC drive cycles using the electro-thermal cell model described in [32]. The electrical model of the LFP prismatic cell is represented by an equivalent circuit model (ECM) with three RC pairs and all the electrical parameters are dependent on both state of charge (SOC) and temperature (T) of the cell. The thermal model takes SOC calculated from the Coulomb counting method, ambient temperature and discharging/charging current from the test as its inputs. The model includes a heat generation model which calculates both the irreversible and the reversible losses. The parameters from the ECM are used to calculate the irreversible heat loss. The reversible loss is calculated using a 2-D look table of entropic coefficients obtained from potentiometric experiment. The cumulative results of both the irreversible and the reversible losses are fed to the first order thermal model of the cell. The surface temperature of the cell which is the output of this thermal model is compared with the measured values of surface temperature of the cell.

The cell has been kept at a constant temperature of 20 °C in a temperature chamber, but the temperature chamber has fluctuations of ±0.5 °C as shown in Fig. 7. The drive cycle current profile which has both charging and discharge currents is applied to the cell from 90%–0% SOC with 20 min breaks in between the cycles. The temperature at the larger surface of the cell is recorded. From Fig. 7, we can clearly observe that from 90% to 0% the model is closely matching with that of the experiment. The RMS error between the experimentally measured surface temperature and the estimated surface temperature from the model is given in Table 8. The estimated temperature from the model using three sets of values for $C_{p_{cell}}$ and R_{cell} show similar RMSE error and are on an average of 0.09 °C and 0.06 °C for WLTC and NEDC drive cycles, respectively. These validation tests prove that $C_{p_{cell}}$ and R_{cell}

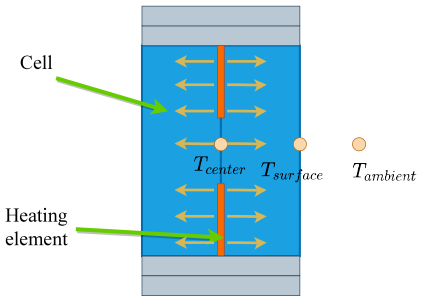

(a) Modified setup of the first order thermal system for validation test [34].

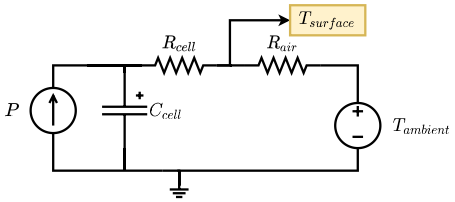

(b) First order thermal model.

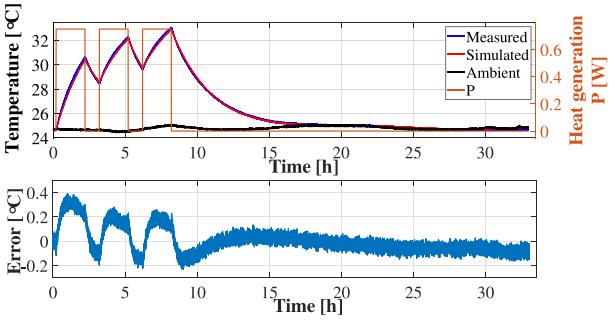

(c) Comparison between the measured and the modelled surface temperature. $C_{p_{cell}} = 1037.56\,\mathrm{JK^{-1}kg^{-1}}$ and $R_{cell} = 0.76\,\mathrm{KW^{-1}}$ are used in the model.

Fig. 6. Test setup, modeling and the results of validation tests.

Table 7
Maximum and RMS error between the model and the experiment for three different cases. The mean values of $C_{p_{cell}}$ and R_{cell} of three trials for 1.2 W, 1.6 W and 2 W are used.

$C_{p_{cell}}$ [J K^{-1} kg^{-1}]	R_{cell} [K W^{-1}]	R_{out} [K W^{-1}]	Max (|Error|) [°C]	RMSE [°C]
1037.56	0.76	14.28	0.39	0.11
1044.73	0.75	14.28	0.41	0.11
1044.05[a]	0.75[a]	14.28	0.40	0.11

[a]Excluding the without lid experimental result.

Table 8
RMS error between the model and the drive cycle test experiment for three different cases. The mean values of $C_{p_{cell}}$ and R_{cell} of three trials for 1.2 W, 1.6 W and 2 W are used.

$C_{p_{cell}}$ [J K^{-1} kg^{-1}]	R_{cell} [K W^{-1}]	R_{out} [K W^{-1}]	WLTC RMSE [m°C]	NEDC RMSE [m°C]
1037.56	0.76	1.61	89.20	62.80
1044.73	0.75	1.61	89.00	62.60
1044.05[a]	0.75[a]	1.61	89.00	62.70

[a]Excluding the without lid experimental result.

calculated using this new method can be used to model the temperature of the lithium-ion cell under various operating conditions.

8. Conclusions

A new method is proposed in this paper to determine the specific heat capacity of pouch and prismatic lithium-ion cells. This new method uses cheap and easily available equipment. No special or expensive equipment like battery cycler, environment chamber, vacuum chamber or calorimeter are required for this method. All the thermal parameters of the cell can be determined from a single experiment thereby making it a time effective one. First a thermal circuit for the setup is developed, then heat transfer equations for the thermal circuit are solved to get a second order differential equation in terms of the insulation temperature. The second order differential equation is solved using the Laplace and the inverse Laplace technique and the final expression for the insulation temperature is used for fitting of the experimental data. A new algorithm is developed to extract

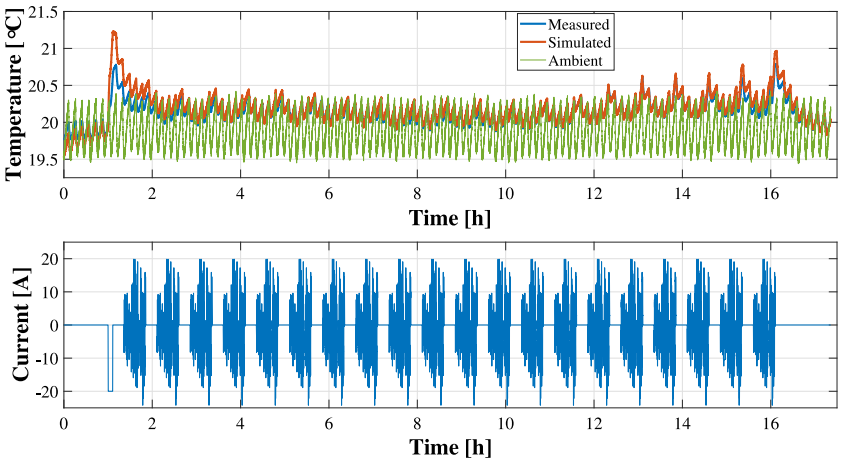

(a) Validation test for WLTC test cycle.

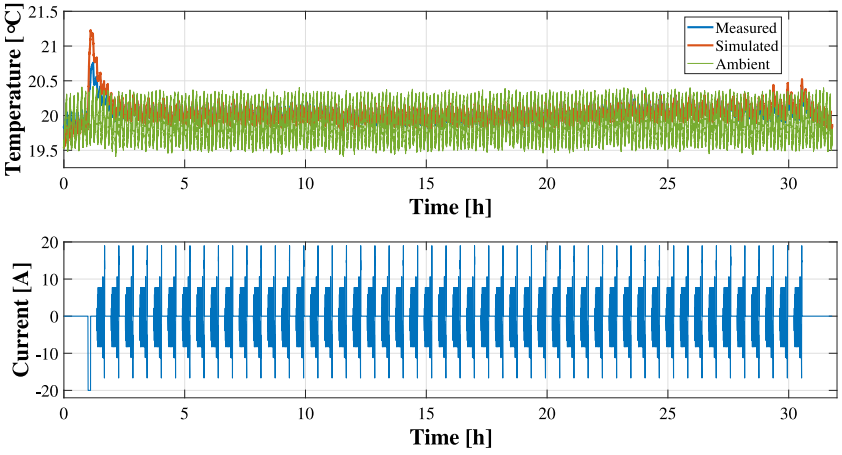

(b) Validation test for NEDC test cycle.

Fig. 7. Validation test for NEDC and WLTC drive cycles. Comparison of the surface temperature from the experiment and the model simulation. $C_{P_{cell}} = 1037.56\,\mathrm{J\,K^{-1}\,kg^{-1}}$ and R_{cell}=0.76 $\mathrm{K\,W^{-1}}$ are used in the thermal model for both the simulations.

the correct value of the specific heat capacity from the fitting results. Experiments are done at three different applied power levels for each of the cells. From the experimental results it can be concluded that only one experiment at a single power is sufficient to obtain satisfactory value of the specific heat capacity. The error can be reduced if more experiments are done for a fixed power. The specific heat capacity results obtained from this method are compared with the results from the calorimetric experiment. The maximum absolute error in the calculated specific heat capacity for the prismatic cell is 1.4% and 5% for the pouch cell. This new method will bring down the time and the cost involved in the thermal characterization of pouch and prismatic lithium ion cells without compromising the measurement accuracy. The thermal parameters obtained from this method can be used to model the surface temperature of a cell under various scenarios. This point has been proved by conducting two validation tests on the prismatic cell. One of the validation tests involves applying an external pulsed power to the cell. In the second validation test the cell is heated up internally using currents from WLTC and NEDC drive cycles. The experimentally measured and the modeled surface temperature of the cell on comparison show excellent agreement.

CRediT authorship contribution statement

Shrisha Balkur: Conceptualization, Methodology, Software, Investigation, Data curation, Visualization, Formal analysis, Validation, Writing - original draft, Writing - review & editing. **Niladri Roy Chowdhury:** Conceptualization, Methodology, Investigation, Data curation, Formal analysis, Validation, Writing - original draft, Writing - review & editing, Project administration. **Jens Groot:** Investigation, Data curation, Resources, Writing - original draft, Visualization. **Torbjörn Thiringer:** Funding acquisition, Project administration, Resources, Supervision, Writing - review & editing.

Declaration of competing interest

The authors declare that they have no known competing financial interests or personal relationships that could have appeared to influence the work reported in this paper.

Acknowledgments

NRC and TT would like to thank Energimyndigheten (P45538-1) and Chalmers Area of Advance Transport for the financing of this work. SB and NRC thank Zeyang Geng, Department of Electrical Engineering, Division of Electric Power Engineering, Chalmers University of Technology, Gothenburg, Sweden for her technical support and suggestions. SB wants to thank Volvo buses for their constant support. Lastly, we would like to thank the battery lab at Volvo GTT for supporting with calorimetric measurements.

Appendix A. Supplementary data

Supplementary material related to this article can be found online at https://doi.org/10.1016/j.jpowsour.2021.229981.

References

[1] A. Schmidt, A. Smith, H. Ehrenberg, Power capability and cyclic aging of commercial, high power lithium ion battery cells with respect to different cell designs, J. Power Sources 425 (2019) 27–38.

[2] A. Kraytsberg, Y. Ein-Eli, Higher, stronger, better…a review of 5 volt cathode materials for advanced lithium-ion batteries, Adv. Energy Mater. 2 (8) (2012) 922–939.

[3] D. Bernardi, E. Pawlikowski, J. Newman, A general energy balance for battery systems, J. Electrochem. Soc. 132 (1) (1985) 5.

[4] L. Song, J.W. Evans, Electrochemical-thermal model of lithium polymer batteries, J. Electrochem. Soc. 147 (6) (2000) 2086.

[5] F. Feng, S. Teng, K. Liu, J. Xie, Y. Xie, B. Liu, K. Li, Co-estimation of lithium-ion battery state of charge and state of temperature based on a hybrid electrochemical-thermal-neural-network model, J. Power Sources 455 (2020) 227935.

[6] P. Gambhire, N. Ganesan, S. Basu, K.S. Hariharan, S.M. Kolake, T. Song, D. Oh, T. Yeo, S. Doo, A reduced order electrochemical thermal model for lithium ion cells, J. Power Sources 290 (2015) 87–101.

[7] Y.-w. Pan, Y. Hua, S. Zhou, R. He, Y. Zhang, S. Yang, X. Liu, Y. Lian, X. Yan, B. Wu, A computational multi-node electro-thermal model for large prismatic lithium-ion batteries, J. Power Sources 459 (2020) 228070.

[8] H. Ruan, J. Jiang, B. Sun, W. Gao, L. Wang, W. Zhang, Online estimation of thermal parameters based on a reduced wide-temperature-range electro-thermal coupled model for lithium-ion batteries, J. Power Sources 396 (2018) 715–724.

[9] D. Ren, X. Feng, L. Lu, M. Ouyang, S. Zheng, J. Li, X. He, An electrochemical-thermal coupled overcharge-to-thermal-runaway model for lithium ion battery, J. Power Sour. 364 (2017) 328–340.

[10] X. Feng, L. Lu, M. Ouyang, J. Li, X. He, A 3D thermal runaway propagation model for a large format lithium ion battery module, Energy 115 (2016) 194–208.

[11] X. Cui, J. Zeng, H. Zhang, J. Yang, J. Qiao, J. Li, W. Li, Optimization of the lumped parameter thermal model for hard-cased li-ion batteries, J. Energy Storage 32 (2020) 101758.

[12] X. Lin, H.E. Perez, S. Mohan, J.B. Siegel, A.G. Stefanopoulou, Y. Ding, M.P. Castanier, A lumped-parameter electro-thermal model for cylindrical batteries, J. Power Sources 257 (2014) 1–11.

[13] A. Greco, D. Cao, X. Jiang, H. Yang, A theoretical and computational study of lithium-ion battery thermal management for electric vehicles using heat pipes, J. Power Sources 257 (2014) 344–355.

[14] A. Samba, N. Omar, H. Gualous, Y. Firouz, P. Van den Bossche, J. Van Mierlo, T.I. Boubekeur, Development of an advanced two-dimensional thermal model for large size lithium-ion pouch cells, Electrochim. Acta 117 (2014) 246–254.

[15] G. Guo, B. Long, B. Cheng, S. Zhou, P. Xu, B. Cao, Three-dimensional thermal finite element modeling of lithium-ion battery in thermal abuse application, J. Power Sources 195 (8) (2010) 2393–2398.

[16] S. Goutam, A. Nikolian, J. Jaguemont, J. Smekens, N. Omar, P.V.D. Bossche, J. Van Mierlo, Three-dimensional electro-thermal model of Li-ion pouch cell: Analysis and comparison of cell design factors and model assumptions, Appl. Thermal Eng. 126 (2017) 796–808.

[17] N.S. Spinner, R. Mazurick, A. Brandon, S.L. Rose-Pehrsson, S.G. Tuttle, Analytical, numerical and experimental determination of thermophysical properties of commercial 18650 LiCoO2 lithium-ion battery, J. Electrochem. Soc. 162 (14) (2015) A2789.

[18] H. Maleki, S. Al Hallaj, J.R. Selman, R.B. Dinwiddie, H. Wang, Thermal properties of lithium-ion battery and components, J. Electrochem. Soc. 146 (3) (1999) 947.

[19] Y. Saito, K. Kanari, K. Takano, T. Masuda, A calorimetric study on a cylindrical type lithium secondary battery by using a twin-type heat conduction calorimeter, Thermochim. Acta 296 (1–2) (1997) 75–85.

[20] L. Sheng, L. Su, H. Zhang, Y. Fang, H. Xu, W. Ye, An improved calorimetric method for characterizations of the specific heat and the heat generation rate in a prismatic lithium ion battery cell, Energy Convers. Manage. 180 (2019) 724–732.

[21] A. Lidbeck, K.R. Syed, Experimental Characterization of Li-ion Battery Cells for Thermal Management in Heavy Duty Hybrid Applications, Göteborg, Sweden, 2017.

[22] Y. Tang, T. Li, X. Cheng, Review of specific heat capacity determination of lithium-ion battery, Energy Procedia 158 (2019) 4967–4973.

[23] C. Forgez, D.V. Do, G. Friedrich, M. Morcrette, C. Delacourt, Thermal modeling of a cylindrical LiFePO4/graphite lithium-ion battery, J. Power Sources 195 (9) (2010) 2961–2968.

[24] M. Fleckenstein, S. Fischer, O. Bohlen, B. Bäker, Thermal impedance spectroscopy-A method for the thermal characterization of high power battery cells, J. Power Sources 223 (2013) 259–267.

[25] J.P. Schmidt, D. Manka, D. Klotz, E. Ivers-Tiffée, Investigation of the thermal properties of a Li-ion pouch-cell by electrothermal impedance spectroscopy, J. Power Sources 196 (19) (2011) 8140–8146.

[26] M. Swierczynski, D.I. Stroe, T. Stanciu, S.K. Kær, Electrothermal impedance spectroscopy as a cost efficient method for determining thermal parameters of lithium ion batteries: Prospects, measurement methods and the state of knowledge, J. Cleaner Prod. 155 (2017) 63–71.

[27] S. Drake, D. Wetz, J. Ostanek, S. Miller, J. Heinzel, A. Jain, Measurement of anisotropic thermophysical properties of cylindrical Li-ion cells, J. Power Sources 252 (2014) 298–304.

[28] T.S. Bryden, B. Dimitrov, G. Hilton, C.P. de León, P. Bugryniec, S. Brown, D. Cumming, A. Cruden, Methodology to determine the heat capacity of lithium-ion cells, J. Power Sources 395 (2018) 369–378.

[29] K. Murashko, J. Pyrhönen, J. Jokiniemi, Determination of the through-plane thermal conductivity and specific heat capacity of a Li-ion cylindrical cell, Int. J. Heat Mass Transfer 162 (2020) 120330.

[30] X. Zhang, R. Klein, A. Subbaraman, S. Chumakov, X. Li, J. Christensen, C. Linder, S.U. Kim, Evaluation of convective heat transfer coefficient and specific heat capacity of a lithium-ion battery using infrared camera and lumped capacitance method, J. Power Sources 412 (2019) 552–558.

[31] T.L. Bergman, F.P. Incropera, D.P. DeWitt, A.S. Lavine, Fundamentals of Heat and Mass Transfer, John Wiley & Sons, 2011.

[32] S. Balkur, Electro-thermal modelling of LFP prismatic cell along with the SOC estimation model (Master's thesis), Department of Electrical Engineering, Chalmers University of Technology, Göteborg, Sweden, 2020, https://hdl.handle.net/20.500.12380/301841.

[33] E. Ramírez-Laboreo, C. Sagüés, S. Llorente, Thermal modeling, analysis and control using an electrical analogy, in: 22nd Mediterranean Conference on Control and Automation, IEEE, 2014, pp. 505–510.

[34] O. Almanza, M. Rodríguez-Pérez, J. De Saja, Measurement of the thermal diffusivity and specific heat capacity of polyethylene foams using the transient plane source technique, Polymer Int. 53 (12) (2004) 2038–2044.

[35] Mathworks, Curve fitting toolbox, 2020, https://www.mathworks.com/products/optimization.html.

[36] L. Wadsö, J. Groot, Versatile and cost-effective calorimeter for Li-ion cells, (2021) in preparation.